

Explicit Multimodal Graph Modeling for Human-Object Interaction Detection

Wenxuan Ji¹ Haichao Shi¹ Xiao-Yu zhang¹

¹ Institute of Information Engineering, Chinese Academy of Sciences

Abstract

Transformer-based methods have recently become the prevailing approach for Human-Object Interaction (HOI) detection. However, the Transformer architecture does not explicitly model the relational structures inherent in HOI detection, which impedes the recognition of interactions. In contrast, Graph Neural Networks (GNNs) are inherently better suited for this task, as they explicitly model the relationships between human-object pairs. Therefore, in this paper, we propose **Multimodal Graph Network Modeling (MGNM)** that leverages GNN-based relational structures to enhance HOI detection. Specifically, we design a multimodal graph network framework that explicitly models the HOI task in a four-stage graph structure. Furthermore, we introduce a multi-level feature interaction mechanism within our graph network. This mechanism leverages multi-level vision and language features to enhance information propagation across human-object pairs. Consequently, our proposed MGNM achieves state-of-the-art performance on two widely used benchmarks: HICO-DET and V-COCO. Moreover, when integrated with a more advanced object detector, our method demonstrates a significant performance gain and maintains an effective balance between rare and non-rare classes.

Introduction

Human-object interaction detection is a task that aims to localize human-object pairs and simultaneously infer the interactions between them. This task represents a more profound level of visual scene understanding than standard object detection. A detected HOI instance is represented as a triplet in the form of (human, action, object). Recently, HOI detection has garnered significant attention from the computer vision community, owing to its extensive applications in downstream tasks such as action recognition (Kong and Fu 2022), image caption (Hossain et al. 2018), and visual scene understanding (Ma et al. 2024a).

Similar to object detectors, HOI detectors can be categorized into two primary types: one-stage and two-stage methods. Recent one-stage methods usually employ the Transformer architecture. Specifically, these methods often adapt DETR-like frameworks (Carion et al. 2020) to detect human-object pairs and predict the interactions in parallel via Transformer decoders (Liao et al. 2022; Zhou et al. 2022). However, compared with two-stage methods, one-

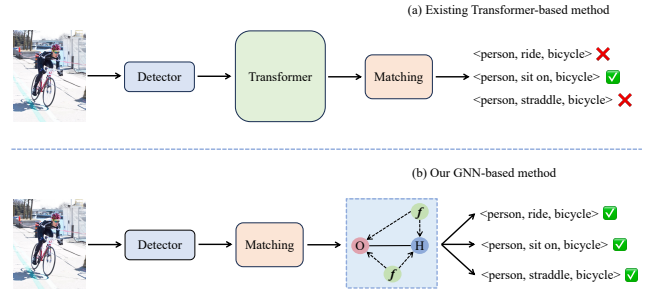


Figure 1: **Comparison of existing Transformer-based methods and our GNN-based method.** Transformer-based methods typically perform feature extraction prior to matching without explicit relational modeling, making it difficult for them to identify complex interactions. In contrast, our GNN-based method firstly constructs human-object pairs via a general matching mechanism and then applies multi-level feature interaction mechanism to enable explicit GNN-based relational reasoning. H, O, and f denote human, object, and multimodal features, respectively.

stage methods cannot easily leverage the features from object detectors, potentially limiting their performance.

Two-stage methods typically follow a distinct training paradigm, which generally involves fine-tuning a pre-trained object detector and subsequently freezing its parameters (Zhang, Campbell, and Gould 2022; Zhang et al. 2023). This paradigm allows the interaction predictor to focus solely on interaction prediction, thereby improving training efficiency. As illustrated in Figure 1(a), recent two-stage methods usually adopt Transformer to extract the visual features. However, **the attention mechanism inherent in the Transformer updates features via a weighted-sum aggregation, which does not explicitly model the relational structure in HOI detection and thus hinders further performance gains.** Motivated by this limitation, we propose a multimodal graph network framework designed to explicitly model the HOI detection task, which more closely aligns with the human perception of HOI.

As illustrated in Figure 1(b), our GNN-based method begins by matching detected human and object instances to construct explicit relational connections for each human-

object pair. Notably, as observed in prior studies (Zhang, Campbell, and Gould 2021; Park, Park, and Lee 2023), relying solely on the visual features of human and object nodes often fails to capture fine-grained contextual cues. Inspired by the success of Vision Language Models (VLMs) (Lei, Wang, and Tan 2024; Guo et al. 2024), we leverage CLIP (Radford et al. 2021) to generate rich multimodal features, thereby enhancing feature interaction between each human-object pair. Benefiting from the sufficient prior knowledge of CLIP, our method not only achieves a significant performance gain but also effectively mitigates the performance disparity between rare and non-rare classes, which is a persistent challenge for previous methods (Zhang, Campbell, and Gould 2021, 2022; Liao et al. 2020). Moreover, we introduce a Multi-level Feature Interaction (MFI) mechanism designed to further utilize these multimodal features and enhance the exchange of contextual information. This mechanism leverages both low-level and high-level vision and language features to intensify the interaction between human-object pairs, thereby enriching the graph network with more fine-grained semantic information.

In light of the preceding analysis, we propose Multimodal Graph Network Modeling (MGNM), a novel and efficient two-stage framework for HOI detection. Our MGNM achieves state-of-the-art performance on two widely used benchmarks: HICO-DET (Chao et al. 2018) and V-COCO (Gupta and Malik 2015). Furthermore, when integrated with a stronger object detector, our method demonstrates a significant performance gain and maintains an effective balance between rare and non-rare classes. The effectiveness of each proposed component is validated through extensive ablation studies. The contributions of this work are as follows:

- We propose a novel multimodal graph network framework that explicitly models the relational structure in HOI detection, addressing the limitations of Transformer-based HOI detectors that rely on implicit attention mechanisms.
- We design a multi-level feature interaction mechanism that effectively fuses low-level and high-level semantic cues across modalities, substantially enhancing the exchange of fine-grained contextual information within the graph structure.
- Extensive experiments on HICO-DET and V-COCO benchmarks demonstrate that our method not only achieves state-of-the-art performance but also maintains an effective balance between rare and non-rare classes.

Related Work

One-stage Methods

One-stage methods are characterized by their parallel detection of human and object instances and prediction of their corresponding interactions. Early approaches typically relied on heuristics such as human keypoints (Liao et al. 2020) or predefined union boxes (Kim et al. 2020). More recently, Transformer-based architectures have become the dominant paradigm for one-stage HOI detection. For instance, Chen et al. (Chen et al. 2021) employ two separate Transformer de-

coders to predict human and object instances and their interactions in parallel. Similarly, Yang et al. (Yang et al. 2023) leveraged VLMs to extract fine-grained semantic features, which were then processed by two sub-decoders to simultaneously predict HOI triplets. Nevertheless, one-stage methods are often encumbered by significant memory usage and slow convergence speed.

Two-stage Methods

Two-stage methods first employ an off-the-shelf object detector to identify human and object instances, and subsequently predict interactions between the matched human-object pairs. Recent two-stage methods often use Transformer encoders to extract features or enhance attention mechanisms (Zhang, Campbell, and Gould 2022; Zhang et al. 2023). Another line of work (Guo et al. 2024; Lei et al. 2023; Lei, Wang, and Robby T. 2024) has incorporated VLMs for feature refinement, leading to notable accuracy improvements. However, while the Transformer excels as a powerful feature extractor, it does not offer an explicit relational modeling framework for the HOI detection task (Antoun and Asmar 2023). To address this gap, our method employs a multimodal graph network framework instead. Our work is situated within a growing line of GNN-based HOI detectors. For instance, SCG (Zhang, Campbell, and Gould 2021) utilized a GNN to facilitate information exchange between human and object nodes, while ViPLO (Park, Park, and Lee 2023) incorporated features from the CLIP image encoder and ViTPose (Xu et al. 2022) to enrich this interaction. Nevertheless, a key limitation of these methods is their primary reliance on visual features, which overlooks the rich semantic cues offered by multimodal features, thereby limiting their ultimate performance.

Method

This section provides a detailed description of our method. We first elaborate on our multi-level feature interaction mechanism, which is structured into four distinct stages. Subsequently, we present the overall framework of MGNM. An overview of our method is illustrated in Figure 2.

Following the standard two-stage paradigm for HOI detection, we assume that a given image contains m detected humans and n detected objects, resulting in $m \times n$ candidate human-object pairs. Here, we denote $\mathbf{N} \in \mathbb{R}^{(m+n) \times d}$ as the human and object instances, which serves as the node representations in the GNN. The corresponding human and object sets within the human-object pairs are represented as $\mathbf{H} \in \mathbb{R}^{(m \times n) \times d}$ and $\mathbf{O} \in \mathbb{R}^{(m \times n) \times d}$, respectively. d is the dimension of the nodes. Additionally, the features of human-object pairs are denoted as $\mathbf{E} \in \mathbb{R}^{(m \times n) \times 2d}$, which can be interpreted as the edge embeddings within the GNN framework.

Multi-level Feature Interaction Mechanism

In this paper, we propose a novel Multi-level Feature Interaction (MFI) mechanism. This mechanism utilizes the low-level and high-level vision and language features to enhance

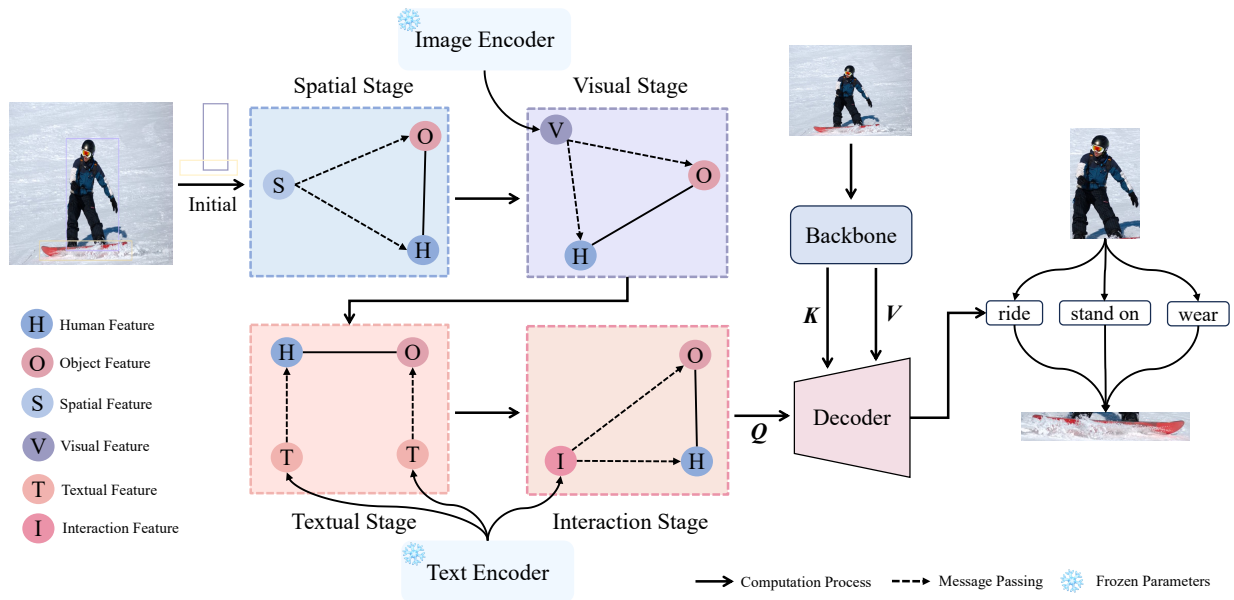


Figure 2: **Overview of our MGNM framework.** The proposed MGNM framework initiates by employing the DETR model to detect human and object instances, which are subsequently matched to form candidate human-object pairs. The features of these pairs are then processed through a four-stage multimodal graph network, consisting of the spatial, visual, textual, and interaction stages. (1) Spatial Stage: For each candidate pair, low-level spatial features derived from their bounding boxes are used to initialize pairwise representations. Simultaneously, these spatial features are utilized to construct a weighted adjacency matrix that regulates feature interactions in the subsequent stages. (2) Visual Stage: High-level visual semantic features are extracted using the CLIP image encoder. These features further enrich the interactions among human-object pairs by incorporating detailed visual context. (3) Textual Stage: The CLIP text encoder is adopted to obtain semantic embeddings for the corresponding human and object categories, providing complementary textual cues for each pair. (4) Interaction Stage: In the final stage, the model captures high-level interaction features between human-object pairs, facilitating more effective relational reasoning within the graph structure. Finally, the refined pairwise representations are utilized as queries in a Transformer decoder, which attends to global image features from the backbone (serving as keys and values), to predict the final HOI triplets.

the interactive modeling of human-object pairs. As illustrated in Figure 2, the MFI mechanism is structured into four sequential stages: Spatial, Visual, Textual, and Interaction. The details of each stage are elaborated below.

Spatial Stage The spatial stage is designed to exploit geometric relationships to enhance interactions between human-object pairs. Specifically, the spatial features comprise bounding box coordinates, box areas, Intersection over Union (IoU), and other related metrics (Zhang, Campbell, and Gould 2021). These features encode the fundamental geometric configurations of each human-object pair and serve as a source of low-level visual information. Moreover, since these are handcrafted features, their computation incurs minimal overhead for the model (Zhang, Campbell, and Gould 2022). Upon extracting the spatial features, we utilize a Multimodality Fusion (MMF) mechanism (Zhang et al. 2023) to integrate them with the initial human and object features, thereby generating the initial representation for each human-object pair.

$$\mathbf{E} = \text{MMF}(\mathbf{H} \oplus \mathbf{O}, \mathbf{S}), \quad (1)$$

where \oplus means the concatenation operation and \mathbf{S} means the spatial features. In addition, based on the spatial features and

corresponding human and object features, the weight matrix \mathbf{W}_G for the multimodal graph network is attained with the multi-branch fusion (MBF) mechanism (Zhang, Campbell, and Gould 2021).

$$\mathbf{W}_G = \text{Linear}(\text{MBF}(\mathbf{H} \oplus \mathbf{O}, \mathbf{S})), \quad (2)$$

where the linear layer is used to align the dimensions.

Visual Stage The visual stage leverages the CLIP to incorporate high-level vision features. Specifically, we employ the CLIP image encoder to extract high-level visual semantic features from the given image. These visual features are then used to pass the high-level visual semantic information to the humans and objects as follows:

$$\mathbf{M}_{\mathcal{V} \rightarrow \mathcal{N}}(\mathbf{V}, \mathbf{N}) = \sigma(\mathbf{W}_G \odot \text{MBF}_v(\mathbf{V}, \mathbf{N})), \quad (3)$$

where $\mathbf{M}_{\mathcal{V} \rightarrow \mathcal{N}}$ denotes the message passing function responsible for propagating visual information to the human and object node features. \mathbf{V} represents the visual features from CLIP. σ is ReLU activation function and \odot is element-wise multiplication. MBF_v is a subclass of the MBF mechanism, tasked with integrating visual and node features. Finally, the human and object node features are updated using a layer normalization step, as formulated below:

$$\mathbf{N} = \text{LN}(\mathbf{N} + \mathbf{M}_{\mathcal{V} \rightarrow \mathcal{N}}(\mathbf{V}, \mathbf{N})), \quad (4)$$

Algorithm 1: Computation Process of Interaction Prediction

Input: $\mathbf{N}, \mathbf{H}, \mathbf{O}$, Image**Output:** Decoder($\mathbf{Q}, \mathbf{K}, \mathbf{V}$)

```
1:  $\mathbf{E} = \text{MMF}(\mathbf{H} \oplus \mathbf{O}, \mathbf{S})$ 
2: for  $i = 1 : T$  do
3:    $\mathbf{W}_G = \text{Linear}(\text{MBF}(\mathbf{H} \oplus \mathbf{O}, \mathbf{S}))$ 
4:    $\mathbf{N} = \text{LN}(\mathbf{N} + \text{M}_{\mathcal{V} \rightarrow \mathcal{N}}(\mathbf{V}, \mathbf{N}))$ 
5:    $\mathbf{N} = \text{LN}(\mathbf{N} + \text{M}_{\mathcal{T} \rightarrow \mathcal{N}}(\mathbf{T}, \mathbf{N}))$ 
6:    $\mathbf{E} = \text{LN}(\text{LN}(\mathbf{E} + \mathbf{H} \oplus \mathbf{O}) + \mathbf{I})$ 
7: end for
8:  $\mathbf{Q} = \mathbf{E}; \mathbf{K}, \mathbf{V} = \text{Backbone}(\text{Image})$ 
9: return Decoder( $\mathbf{Q}, \mathbf{K}, \mathbf{V}$ )
```

where LN means the layer normalization.

Textual Stage The textual stage is dedicated to generating textual embeddings for each node, providing a source of low-level language features. As illustrated in Figure 2, we adopt the prompt template “a photo of a $\langle \text{object} \rangle$ ”, where the $\langle \text{object} \rangle$ comes from the detection results. In this paper, for brevity, we denote the humans and objects as the whole node set \mathbf{N} , and the corresponding textual features are assumed to be matched. The process is formulated as follows:

$$\text{M}_{\mathcal{T} \rightarrow \mathcal{N}}(\mathbf{T}, \mathbf{N}) = \sigma(\mathbf{W}_G \odot \text{MBF}_t(\mathbf{T}, \mathbf{N})), \quad (5)$$

where $\text{M}_{\mathcal{T} \rightarrow \mathcal{N}}$ means the message passing function responsible for propagating textual information to the human and object node features. \mathbf{T} means the textual features from CLIP. MBF_t is a subclass of the MBF mechanism. Similarly, we also use layer normalization step when updating the human and object features.

$$\mathbf{N} = \text{LN}(\mathbf{N} + \text{M}_{\mathcal{T} \rightarrow \mathcal{N}}(\mathbf{T}, \mathbf{N})). \quad (6)$$

Interaction Stage To incorporate high-level interaction semantic cues, we again employ the CLIP text encoder. This time, it is used to generate interaction-centric semantic features, which constitute high-level language features. The prompt template “a photo of a person interacting with $\langle \text{object} \rangle$ ” is adopted, which aims to boost the feature interaction between human-object pairs. This process is formulated as follows:

$$\mathbf{E} = \text{LN}(\mathbf{E} + \mathbf{I}), \quad (7)$$

where \mathbf{I} denotes the interaction features of the human-object pairs. As a preliminary step, the human-object pair features are first enriched by integrating the features of their corresponding human and object nodes as follows:

$$\mathbf{E} = \text{LN}(\mathbf{E} + \mathbf{H} \oplus \mathbf{O}). \quad (8)$$

Multimodal Graph Network Modeling

Building upon the MFI mechanism detailed above, this section presents the complete architecture of the proposed MGNM framework.

As illustrated in Figure 2, the process begins with an off-the-shelf object detector, which extracts bounding boxes and appearance features. Based on these detection results and a

matching strategy, we construct human and object instances \mathbf{N} , along with human features \mathbf{H} and object features \mathbf{O} . At the core of our framework lies the MFI mechanism, as detailed in Algorithm 1 (Lines 1–7). The process commences by constructing the initial human-object pair features, which are then iteratively refined through the proposed four-stage pipeline. Following (Park, Park, and Lee 2023), we set the number of iterative steps T to 2. Notably, in the visual and textual stages, we leverage visual and textual features to update the human and object instances, thereby infusing multimodal information into the node encodings. In addition, since the message passing is guided by a weight matrix computed from the relational structure among human-object pairs, this implicitly promotes feature interaction between pairs. In contrast, the spatial and interaction stages are explicitly designed to enhance feature communication between human-object pairs. Finally, a decoder is employed to incorporate contextual semantic information and produce the final predictions. In this decoder, the human-object pair features act as queries, while the global features extracted from the backbone serve as keys and values.

Experiments

This section presents a series of experiments designed to evaluate the effectiveness of our proposed method. First, we briefly introduce the experimental settings. Next, we present a comprehensive comparison of our method against existing state-of-the-art methods. Subsequently, the ablation study of our method is conducted. Finally, we rethink and analyze the Rare-Non-rare bias in the HOI detection field and provide some promising suggestions.

Experimental Settings

Datasets Our experiments are conducted on two widely used public benchmarks: HICO-DET and V-COCO. HICO-DET contains 38,118 training images and 9,658 test images. It includes 80 object classes from the MS COCO dataset (Lin et al. 2014) and 117 action classes, which combine to form 600 types of HOI instances. V-COCO, a smaller-scale subset of the MS COCO dataset, contains 2,533 training, 2,867 validation, and 4,946 test images, encompassing 80 object classes and 29 action classes. Given its larger scale and closer alignment with real-world data distributions, our primary experimental focus is on the HICO-DET dataset.

Evaluation Metrics Following the standard evaluation protocols in (Park, Park, and Lee 2023), we report the mean Average Precision (mAP) for evaluation. An HOI triplet is considered a true positive when the IoU of the detected human and object is larger than 0.5 and the action is predicted accurately. For the HICO-DET dataset, we report performance under two standard evaluation settings: Default and Known Object. Each setting has three different subsets: (1) all 600 HOI classes (Full), (2) 138 HOI classes with less than 10 training instances (Rare), and (3) 462 HOI classes with 10 or more training instances (Non-Rare). For the V-COCO dataset, we evaluate performance based on two scenarios: Scenario 1, which requires correct prediction of occluded object bounding boxes, and Scenario 2, which does not.

Method	Backbone	HICO-DET						V-COCO	
		Default			Known Object			AP_{role}^{S1}	AP_{role}^{S2}
		Full	Rare	Non-Rare	Full	Rare	Non-Rare		
<i>One-stage methods</i>									
UnionDet (2020)	R50-F	17.58	11.72	19.33	19.76	14.68	21.27	47.5	56.2
PPDM (2024)	Swin-B-F	27.59	18.07	30.44	29.11	18.85	32.71	-	-
AS-Net (2021)	R50	28.87	24.25	30.25	31.74	27.07	33.14	53.9	-
FGAHOI-S (2024b)	Swin-T	29.94	22.24	32.24	32.48	24.16	34.97	60.5	61.2
DOQ (2022)	R50+C	33.28	29.19	34.50	-	-	-	63.5	-
GEN-VLTK (2022)	R50+C	33.75	29.25	35.10	36.78	32.75	37.99	62.4	64.4
DiffHOI-S (2023)	R50+C+SD	34.41	31.07	35.40	37.31	34.56	38.14	61.1	63.5
FGAHOI-L (2024b)	Swin-L	37.18	30.71	39.11	38.93	31.93	41.02	-	-
DiffHOI-L (2023)	Swin-L+C+SD	40.63	38.10	41.38	43.14	40.24	44.01	<u>65.7</u>	68.2
<i>Two-stage methods</i>									
SCG (2021)	R50-F	29.26	24.61	30.65	32.87	27.89	34.35	54.2	60.9
PPDM++ (2024)	Swin-B-F	30.10	23.73	32.00	31.80	24.93	33.85	-	-
UPT (2022)	R101	32.31	28.55	33.44	35.65	31.60	36.86	60.7	66.2
ADA-CM (2023)	R50+C	33.80	31.72	34.42	-	-	-	60.7	66.2
ILCN (2025)	Swin-T	33.80	29.83	34.99	-	-	-	63.4	65.3
PViC w/ DETR (2023)	R50	34.69	32.14	35.45	38.14	35.38	38.97	62.8	67.8
HOIGen (2024)	R50+C	34.84	34.52	34.94	-	-	-	-	-
ViPLO (2023)	R101-D+C+VP	34.95	33.83	35.28	38.15	36.77	38.56	60.9	66.6
TKCE (2025)	R50+C	35.11	34.35	35.34	-	-	-	-	-
LAIN (2025)	R50+C	36.02	35.70	36.11	-	-	-	63.4	65.3
MP-HOI-S (2024)	R50+C+SD	36.50	35.48	36.80	-	-	-	66.2	67.6
PViC w/ \mathcal{H} -DETR (2023)	Swin-L	44.32	<u>44.61</u>	44.24	<u>47.81</u>	<u>48.38</u>	<u>47.64</u>	64.1	<u>70.2</u>
MP-HOI-L (2024)	Swin-L+C+SD	<u>44.53</u>	44.48	<u>44.55</u>	-	-	-	-	-
MGNM	R50+C	36.68	34.10	37.45	39.99	37.15	40.84	62.1	67.5
MGNM w/ \mathcal{H} -DETR	Swin-L+C	46.54	48.09	46.07	49.78	50.82	49.47	64.3	70.5

Table 1: Performance comparison in terms of mAP (%) on the HICO-DET and V-COCO dataset. To ensure a fair comparison, we report both the performance and the corresponding feature backbone for each method. In each evaluation metric, the best result is marked in bold and the second-best result is underlined. In this paper, R50, R101, R50-F and R101-D denotes ResNet50, ResNet101, ResNe50-FPN and ResNet101-DC5 model, respectively. A similar notation applies to Swin Transformer (Liu et al. 2021). C, SD, and VP mean CLIP, Stable Diffusion, and ViTPose models, respectively. We note that MP-HOI (Yang et al. 2024) utilizes additional training data (Magic-HOI and SynHOI), which should be considered when comparing results.

Implementation Details For HICO-DET and V-COCO datasets, we use the fine-tuned DETR and \mathcal{H} -DETR (Jia et al. 2023) weights provided by Zhang et al. (Zhang et al. 2023). During training, following the commonly used training paradigm of two-stage methods, the weights of the object detector are frozen, while only the interaction predictor is trained. Meanwhile, the focal loss (Lin et al. 2017) is employed as the loss function. Following (Lei et al. 2023), we also incorporate the adapter into the CLIP module. The model is optimized using the AdamW optimizer with an initial learning rate of 10^{-4} . All models are trained for 30 epochs on 4 NVIDIA A100 GPUs, using a total batch size of 32. Unless otherwise specified, all other hyperparameters adhere to the settings established in (Zhang et al. 2023; Lei et al. 2023).

Comparison with State-of-the-art Methods

Table 1 provides a comprehensive performance comparison between our proposed MGNM and current state-of-the-art methods. For clarity, the competing methods are grouped

into one-stage and two-stage categories. On the HICO-DET dataset, MGNM outperforms all other one-stage and two-stage approaches that utilize a ResNet backbone. Specifically, in the Default Full setting, our method achieves a 2.27 mAP improvement over DiffHOI-S, despite the latter leveraging two VLMs, namely CLIP and Stable Diffusion (Romach et al. 2021). MGNM also surpasses the leading two-stage approach, MP-HOI-S, by 0.18 mAP in the Default Full setting, even though MP-HOI-S incorporates both additional VLMs and extra training data. Moreover, MGNM exceeds the performance of the recent GNN-based ViPLO by 1.73 mAP in the Default Full setting, notwithstanding ViPLO’s adoption of the supplementary ViTPose-L model (Xu et al. 2022). In the Known Object setting, MGNM consistently outperforms all ResNet-based counterparts across all three subsets by a substantial margin. Notably, our ResNet50-based MGNM even surpasses FGAHOI-L, which utilizes a more powerful Swin-L backbone, by 1.06 mAP in the Full setting. Collectively, these results demonstrate the effectiveness of our multimodal graph network and its ex-

Methods	Full	Rare	Non-Rare
w/o Spatial Stage	36.00	34.68	36.39
w/o Visual Stage	35.32	32.66	36.12
w/o Textual Stage	36.16	33.81	36.86
w/o Interaction Stage	35.61	33.37	36.28
vanilla	36.68	34.10	37.45

Table 2: Effectiveness of each component within our MFI mechanism. w/o means “without”.

Methods	Backbone	mAP \uparrow	Time \downarrow	Memory \downarrow
SCG	R101	29.26	182 ms	7,702 MiB
ViPLO	R101-D+C+VP	34.95	166 ms	10,224 MiB
MGNM	R50+C	36.68	125 ms	2,946 MiB

Table 3: Comparison of mAP, inference time, and GPU memory on the HICO-DET test set. We select two prominent GNN-based baselines for this comparison: SCG and ViPLO. It is important to note that the official implementations of both SCG and ViPLO execute object detection and interaction prediction as two separate, sequential processes. Therefore, to ensure a fair comparison, our reported time and memory for these baselines encompass the complete process. All experiments are conducted with a batch size of 1 on a single NVIDIA A100 GPU. Time refers to the elapsed time required for processing one image.

explicit modeling strategy for HOI detection. On the V-COCO dataset, MGNM also achieves highly competitive performance among ResNet-based methods. We note that MP-HOI-S obtains a higher AP_{role}^{S1} , which we attribute to its use of additional training data. This observation suggests that GNN-based approaches, including MGNM, could further benefit from large-scale pre-training, highlighting a promising direction for future research.

Furthermore, to further demonstrate the scalability of our approach, we compare the performance of MGNM equipped with a more powerful object detector against other state-of-the-art methods that utilize similarly strong backbones. As shown in Table 1, MGNM integrated with \mathcal{H} -DETR achieves substantial performance improvements over the competing methods. For example, on the HICO-DET Default Full setting, our method outperforms PViC with \mathcal{H} -DETR by 2.22 mAP. Notably, although both DiffHOI-L and MP-HOI-L leverage two VLMs each, our single-VLM approach achieves significant gains of 5.91 and 2.01 mAP over these methods, respectively. These results underscore not only the scalability of our framework but also the effectiveness of our multimodal graph network design.

Ablation Study

In this subsection, we conduct ablation studies to analyse the effectiveness of our proposed components and the efficiency of our MGNM framework. All the experiments are conducted on the HICO-DET test set under Default setting.

Components Analysis We first analyze the contribution of each of the four stages within our MFI mechanism, which collectively process low-level and high-level multimodal features. As shown in Table 2, removing the low-level feature stages, namely the Spatial (row 1) and Textual (row 3) stages, results in performance drops of 0.68 and 0.52 mAP, respectively. This demonstrates that these low-level spatial and textual features provide a valuable supplement to the foundational human-object pair representations. Ablating the high-level feature stages, the Visual (row 2) and Interaction (row 4) stages, induces a more substantial performance degradation, with drops of 1.36 and 1.07 mAP, respectively. These decreases are considerably larger than those observed in low-level stages. This finding suggests that the high-level features are more critical to our model’s predictive power, an observation that aligns with the notion that GNNs are inherently biased towards modeling high-level structural information (Antoun and Asmar 2023). Interestingly, we observe a counter-intuitive phenomenon in row 1: ablating the spatial stage improves performance on the rare classes. This suggests that low-level vision features may inadvertently amplify the model’s existing bias towards more frequent, non-rare classes. Nevertheless, considering their substantial positive impact on the Full and Non-Rare settings, these spatial features remain an indispensable component for overall model performance.

Efficiency Analysis This subsection presents an efficiency analysis of MGNM in comparison to two related GNN-based methods, focusing on inference time and GPU memory usage. As reported in Table 3, both SCG and ViPLO decouple the object detection and interaction prediction processes, whereas our method integrates these stages into a unified end-to-end pipeline. To ensure a fair comparison, we report the total inference time and GPU memory for SCG and ViPLO, excluding file I/O operations. As shown in Table 3, our approach not only achieves substantially higher mAP but also demonstrates superior efficiency, recording the lowest inference time and GPU memory consumption among the compared methods. These results highlight the strong balance between effectiveness and efficiency achieved by MGNM. It is worth noting that the official object detection scripts provided by the baseline methods appear to be unoptimized with respect to memory usage. When replacing their detection modules with DETR weights, resulting in less GPU consumption than the actual GPU memory usage, the measured occupancy drops to 1,904 MiB for SCG and 4,426 MiB for ViPLO. Even under these conditions, when comprehensively considering both mAP and inference time, our method continues to deliver the best overall effectiveness and efficiency.

Rethinking Rare-Non-rare Bias

The challenge of few-shot learning is particularly pronounced in HOI detection, where it manifests as a significant performance disparity between rare and non-rare classes. As evidenced in Table 1, this long-tail distribution problem is severe in many methods. For instance, PPDM and FGAHOI-S exhibit a performance gap of over 10 mAP be-

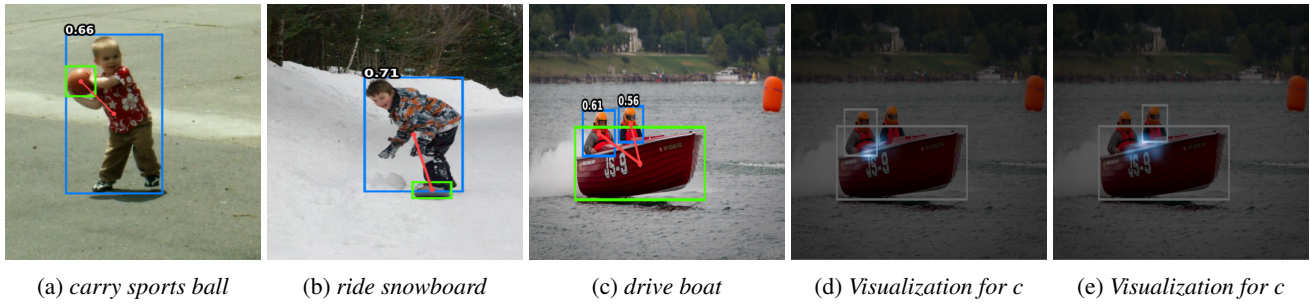


Figure 3: Qualitative results on the HICO-DET test set. Figures 3a and 3b illustrate successful predictions across a variety of challenging scenarios. In contrast, Figure 3c presents a representative failure case, wherein the model generates a false positive triplet. Specifically, it incorrectly infers that both individuals are driving the boat, whereas only the person on the right is performing this action. To further investigate this failure case, Figures 3d and 3e visualize the corresponding attention maps, highlighting the model’s regions of focus that led to this prediction.

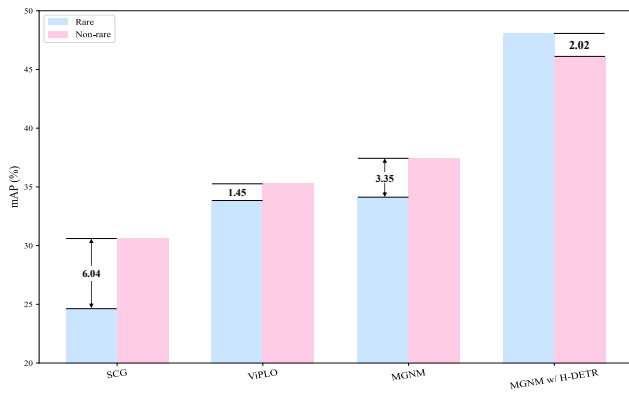


Figure 4: Comparison of our method and two related GNN-based methods on rare and non-rare classes.

tween their rare and non-rare classes. Similarly, in Figure 4, the GNN-based method SCG also has a significant difference between rare and non-rare classes. However, a key observation from Table 1 is that methods incorporating VLMs substantially mitigate this disparity. This suggests that the rich prior knowledge in VLMs can effectively alleviate the Rare-Non-rare bias. Our own results, illustrated in Figure 4, support this hypothesis: both our MGNM and ViPLO, which leverage CLIP, demonstrate a much narrower performance gap between rare and non-rare classes. Interestingly, ViPLO achieves a better balance than our method. We hypothesize that its use of an additional ViTPose-L model provides another source of rich prior knowledge, playing a similar role like VLMs. Moreover, as shown in Table 1 and Figure 4, an unexpected trend emerges for methods equipped with the \mathcal{H} -DETR object detector, these models exhibit a remarkable reversal, where performance on rare classes actually exceeds that on non-rare classes. We posit that this is likely attributable to the unique architectural design of \mathcal{H} -DETR, and a deeper investigation into this phenomenon presents a compelling direction for future research. In summary, our analysis indicates that leveraging VLMs and advanced object detectors represents a highly effective strategy for miti-

gating the Rare-Non-rare bias in HOI detection.

Qualitative Results and Analysis

This section presents a qualitative analysis of our method’s predictions, highlighting both its strengths and current limitations. As illustrated in Figures 3a and 3b, our model demonstrates robustness by accurately predicting HOI triplets even when the target object is small or occluded. Conversely, Figure 3c presents a representative failure case involving a false positive prediction. Here, the model incorrectly infers that two individuals are driving the boat, a prediction that contradicts common sense in the real world. To diagnose this error, we visualize the corresponding attention maps in Figures 3d and 3e. The visualization reveals that the model correctly identifies promising regions associated with the *drive* action for both individuals. However, it lacks the commonsense knowledge to understand that only one person can drive a single boat, leading to the erroneous prediction. Furthermore, attention is diffuse and does not pinpoint fine-grained cues, such as hand-on-wheel placement. This limitation highlights a crucial direction for future work: developing methods to inject real-world commonsense reasoning into HOI detectors to resolve such logical ambiguities.

Conclusion

In this paper, we introduce Multimodal Graph Network Modeling (MGNM), a novel and effective two-stage HOI detection framework. The central contribution of MGNM lies in its explicit modeling of the HOI detection task via the construction of a multimodal graph network. Furthermore, by leveraging Vision Language Models (VLMs), we design a multi-level feature interaction mechanism that systematically fuses low-level and high-level vision and language features, thereby enhancing information propagation within the graph structure. Extensive experiments validate that our approach not only achieves state-of-the-art performance but also delivers superior computational efficiency. In addition, our analysis of the pervasive class imbalance issue provides new insights and practical recommendations for mitigating the Rare-Non-rare bias in future research.

References

- Antoun, M.; and Asmar, D. 2023. Human object interaction detection: Design and survey. *Image and Vision Computing*, 130: 104617.
- Carion, N.; Massa, F.; Synnaeve, G.; Usunier, N.; Kirillov, A.; and Zagoruyko, S. 2020. End-to-End Object Detection with Transformers. *European Conference on Computer Vision*.
- Chao, Y.-W.; Liu, Y.; Liu, X.; Zeng, H.; and Deng, J. 2018. Learning to detect human-object interactions. In *IEEE winter conference on applications of computer vision*, 381–389. IEEE.
- Chen, M.; Liao, Y.; Liu, S.; Chen, Z.; Wang, F.; and Qian, C. 2021. Reformulating HOI Detection as Adaptive Set Prediction. In *IEEE/CVF Conference on Computer Vision and Pattern Recognition*.
- Guo, Y.; Liu, Y.; Li, J.; Wang, W.; and Jia, Q. 2024. Unseen No More: Unlocking the Potential of CLIP for Generative Zero-shot HOI Detection. *ArXiv*, abs/2408.05974.
- Gupta, S.; and Malik, J. 2015. Visual semantic role labeling. *arXiv preprint arXiv:1505.04474*.
- Hossain, M. Z.; Sohel, F.; Shiratuddin, M. F.; and Laga, H. 2018. A Comprehensive Survey of Deep Learning for Image Captioning. *ACM Computing Surveys*, 51: 1 – 36.
- Jia, D.; Yuan, Y.; He, H.; pei Wu, X.; Yu, H.; Lin, W.; huan Sun, L.; Zhang, C.; and Hu, H. 2023. DETRs with Hybrid Matching. *IEEE/CVF Conference on Computer Vision and Pattern Recognition*, 19702–19712.
- Kim, B.; Choi, T.; Kang, J.; and Kim, H. J. 2020. Uniondet: Union-level detector towards real-time human-object interaction detection. In *European Conference on Computer Vision*, 498–514. Springer.
- Kim, S.; Jung, D.; and Cho, M. 2025. Locality-Aware Zero-Shot Human-Object Interaction Detection. In *IEEE/CVF Conference on Computer Vision and Pattern Recognition*, 20190–20200.
- Kong, Y.; and Fu, Y. 2022. Human action recognition and prediction: A survey. *International Journal of Computer Vision*, 130(5): 1366–1401.
- Lei, Q.; Wang, B.; and Robby T., T. 2024. EZ-HOI: VLM Adaptation via Guided Prompt Learning for Zero-Shot HOI Detection. In *The Thirty-eighth Annual Conference on Neural Information Processing Systems*.
- Lei, Q.; Wang, B.; and Tan, R. T. 2024. EZ-HOI: VLM Adaptation via Guided Prompt Learning for Zero-Shot HOI Detection. *ArXiv*, abs/2410.23904.
- Lei, T.; Caba, F.; Chen, Q.; Ji, H.; Peng, Y.; and Liu, Y. 2023. Efficient Adaptive Human-Object Interaction Detection with Concept-guided Memory. In *IEEE/CVF International Conference on Computer Vision*. IEEE.
- Liao, Y.; Liu, S.; Gao, Y.; Zhang, A.; Li, Z.; Wang, F.; and Li, B. 2024. PPDMM++: Parallel Point Detection and Matching for Fast and Accurate HOI Detection. *IEEE Transactions on Pattern Analysis and Machine Intelligence*, 46(10): 6826–6841.
- Liao, Y.; Liu, S.; Wang, F.; Chen, Y.; Qian, C.; and Feng, J. 2020. Ppdm: Parallel point detection and matching for real-time human-object interaction detection. In *IEEE/CVF Conference on Computer Vision and Pattern Recognition*, 482–490.
- Liao, Y.; Zhang, A.; Lu, M.; Wang, Y.; Li, X.; and Liu, S. 2022. GEN-VLKT: Simplify Association and Enhance Interaction Understanding for HOI Detection. *IEEE/CVF Conference on Computer Vision and Pattern Recognition*, 20091–20100.
- Lin, T.-Y.; Goyal, P.; Girshick, R. B.; He, K.; and Dollár, P. 2017. Focal Loss for Dense Object Detection. *IEEE Transactions on Pattern Analysis and Machine Intelligence*, 42: 318–327.
- Lin, T.-Y.; Maire, M.; Belongie, S.; Hays, J.; Perona, P.; Ramanan, D.; Dollár, P.; and Zitnick, C. L. 2014. Microsoft coco: Common objects in context. In *European Conference on Computer Vision*, 740–755. Springer.
- Liu, Z.; Lin, Y.; Cao, Y.; Hu, H.; Wei, Y.; Zhang, Z.; Lin, S.; and Guo, B. 2021. Swin Transformer: Hierarchical Vision Transformer using Shifted Windows. *IEEE/CVF International Conference on Computer Vision*, 9992–10002.
- Lu, M.; Yang, G.; Wang, Y.; and Luo, K. 2025. Intra- and inter-instance location correlation network for human-object interaction detection. *Engineering Applications of Artificial Intelligence*, 142: 109942.
- Ma, F.; Wang, B.; Dong, X.; Li, M.; Ma, H.; Jia, R.; and Jain, A. 2024a. Scene Understanding Method Utilizing Global Visual and Spatial Interaction Features for Safety Production. *Information Fusion*, 102668.
- Ma, S.; Wang, Y.; Wang, S.; and Wei, Y. 2024b. FGAHOI: Fine-Grained Anchors for Human-Object Interaction Detection. *IEEE Transactions on Pattern Analysis and Machine Intelligence*, 46(4): 2415–2429.
- Nan, F.; Zhang, N.; Liu, Q.; Jing, W.; Dai, G.; Chen, Y.; and Tian, F. 2025. Exploring Triple Knowledge Cues for Zero-Shot Human-Object Interaction Detection. In *IEEE International Conference on Acoustics, Speech and Signal Processing*, 1–5.
- Park, J.; Park, J.-W.; and Lee, J.-S. 2023. ViPLO: Vision Transformer based Pose-Conditioned Self-Loop Graph for Human-Object Interaction Detection. *IEEE/CVF Conference on Computer Vision and Pattern Recognition*.
- Qu, X.; Ding, C.; Li, X.; Zhong, X.; and Tao, D. 2022. Distillation using oracle queries for transformer-based human-object interaction detection. In *IEEE/CVF Conference on Computer Vision and Pattern Recognition*, 19558–19567.
- Radford, A.; Kim, J. W.; Hallacy, C.; Ramesh, A.; Goh, G.; Agarwal, S.; Sastry, G.; Askell, A.; Mishkin, P.; Clark, J.; Krueger, G.; and Sutskever, I. 2021. Learning Transferable Visual Models From Natural Language Supervision. In *International Conference on Machine Learning*.
- Rombach, R.; Blattmann, A.; Lorenz, D.; Esser, P.; and Ommer, B. 2021. High-Resolution Image Synthesis with Latent Diffusion Models. *IEEE/CVF Conference on Computer Vision and Pattern Recognition*, 10674–10685.

- Xu, Y.; Zhang, J.; Zhang, Q.; and Tao, D. 2022. ViTPose: Simple Vision Transformer Baselines for Human Pose Estimation. In *Advances in Neural Information Processing Systems*.
- Yang, J.; Li, B.; Yang, F.; Zeng, A.; Zhang, L.; and Zhang, R. 2023. Boosting Human-Object Interaction Detection with Text-to-Image Diffusion Model. *arXiv preprint arXiv:2305.12252*.
- Yang, J.; Li, B.; Zeng, A.; Zhang, L.; and Zhang, R. 2024. Open-World Human-Object Interaction Detection via Multi-Modal Prompts. *IEEE/CVF Conference on Computer Vision and Pattern Recognition*, 16954–16964.
- Zhang, F. Z.; Campbell, D.; and Gould, S. 2021. Spatially Conditioned Graphs for Detecting Human–Object Interactions. In *IEEE/CVF International Conference on Computer Vision*, 13319–13327.
- Zhang, F. Z.; Campbell, D.; and Gould, S. 2022. Efficient Two-Stage Detection of Human-Object Interactions with a Novel Unary-Pairwise Transformer. In *IEEE/CVF Conference on Computer Vision and Pattern Recognition*, 20104–20112.
- Zhang, F. Z.; Yuan, Y.; Campbell, D.; Zhong, Z.; and Gould, S. 2023. Exploring Predicate Visual Context in Detecting Human–Object Interactions. In *IEEE/CVF International Conference on Computer Vision*, 10411–10421.
- Zhou, D.; Liu, Z.; Wang, J.; Wang, L.; Hu, T.; Ding, E.; and Wang, J. 2022. Human-Object Interaction Detection via Disentangled Transformer. *IEEE/CVF Conference on Computer Vision and Pattern Recognition*, 19546–19555.